Chen and Guan *EURASIP Journal on Wireless Communications and Networking* (2020) 2020:154
https://doi.org/10.1186/s13638-020-01766-6

EURASIP Journal on Wireless Communications and Networking

RESEARCH Open Access

Correntropy-based DOA estimation algorithm under impulsive noise environments

Jin Chen* and Sheng Guan*

* Correspondence: cjwoods@163.com; gs-sunny@foxmail.com
Tianjin Key Laboratory of Wireless Communications and Power Transmission, Tianjin Normal University, Tianjin 300387, China

Abstract

In this paper, the direction of arrival (DOA) estimation of signals in the presence of impulsive noise environment is studied. Complex isotropic symmetric alpha-stable (*SaS*) random variables are modeled as impulsive noise, then a novel second-order statistic method that correntropy-based covariance matrix (CBCM) is defined, based on the combination of the CBCM of the array sensor outputs with the signal subspace technique (e.g., multiple signal classification (MUSIC)), which can be achieved source localization under impulsive noise environments. The Monte-Carlo simulation results illustrate the improved performance of CBCM-MUSIC for DOA estimation under a wide range of impulsive noise conditions.

Keywords: Direction of arrival, Correntropy, Complex isotropic symmetric alpha-stable

1 Introduction

Array signal processing is an important branch in modern signal processing. It is widely used in the field of radar [1], sonar [2], 5G communication [3–6], and smart antenna [7]. DOA estimation algorithms under additive white noise have been extensively studied in the past several decades. However, literature [8–11] studies show that atmospheric environments, sea clutter, ground clutter, radar backscatter echoes, and urban mobile radio channels, sudden bursts, or sharp spikes are exhibited at the array outputs which can be characterized as impulsive; an impulsive environment can be well modeled by alpha-stable distribution [12], compared with the mixture Gaussian distribution, and the alpha-stable distribution has "thick tail" statistical characteristics of impulse noise, which makes it have strongly impulse characteristics in the time domain. Second-order statistics are not finite [12] under alpha-stable distribution. In order to suppress these impulsive outliers, researchers have proposed a series of DOA estimation methods based on fractional lower-order statistics (FLOS).

In [13], the authors proposed new subspace methods based on fractional lower-order moment (FLOM) covariance estimates, and the robust covariation-based

MUSIC (ROC-MUSIC) used covariations under the assumption that the signals and the additive noise are jointly $S\alpha S$, which does not hold always because signals of interest are generally of finite variances, and the ROC-MUSIC is defined only for $1 < \alpha < 2$.

In [14], the authors proposed a new class of covariance matrices named FLOM matrices for impulsive noise. The FLOM outperforms the ROC-MUSIC from the fact that it handles all types of signals. However, it is limited in the range of α ($\alpha > 1$) for robust covariation.

In [15], the authors introduce a new subspace algorithm based on the phased fractional lower-order moment (PFLOM), and the new subspace algorithm based on the PFLOM covariance estimation shows a higher resolution capability and lower estimation error.

In [16], the authors proposed a new operator referred to as the correntropy-based correlation (CRCO), and it can be applied with MUSIC algorithm; despite the CRCO-MUSIC shows robustness in highly impulsive noise environments or in low generalized signal to noise ratio (GSNR) situation, the formulation for the robust CRCO statistics needs quite a number of snapshots.

Professor Principe's team first proposed the correntropy in [17]. The correntropy is a new statistic that can quantify the time structure as well as the statistical distribution of two stochastic random processes. The correntropy function conveys information about the quadratic Renyi's entropy of the generating source. At the same time, correntropy can well suppress impulse noise and does not depend on the prior knowledge of alpha-stable noise. Therefore, it has been widely used in signal detection [18], time delay estimation [19], adaptive filtering [17], and image processing [20].

In this paper, we focused on the issue of DOA estimation algorithm in extremely high impulsive noise environments along with low generalized signal to noise ratio (GSNR) levels and fewer snapshots and introduced a new operator based on correntropy, namely, correntropy-based covariance matrices (CBCM), which can be combined with subspace algorithm, such as MUSIC algorithm, that is CBCM-MUSIC algorithm. The CBCM-MUSIC algorithm exhibits an evident performance in low GSNR or in strong impulsive environments.

Our major contributions are listed as follows:

(1) Consider the problem of DOA estimation in impulsive noise and proposes a new method to rebuild the covariance matrix based on correntropy.
(2) Several experiments have been made for the selection of kernel size and suppression parameter.
(3) The performances of different algorithms are compared, and the effectiveness of the proposed method is verified.

The paper is organized as follows: in Section 2, we define the problem of interest and briefly review some preliminaries on α-stable distributions. In Section 3, we provide the CBCM-MUSIC algorithm. Finally, some simulation examples are presented in Section 4, and the conclusion is given in Section 5.

Notation: Lowercase (capital) bold symbols denote vector (matrix). $(\cdot)^{\mathrm{T}}$, $(\cdot)^{*}$, and $(\cdot)^{\mathrm{H}}$ denote transpose, complex conjugation, and conjugate transposition, respectively; E{·} denotes expectation operator; and |·| stands for an absolute value of a random quantity.

2 Problem definition

Here, the array signal model has given in Section 2.1, and then the impulsive noise model (alpha-stable noise) is presented in Section 2.2.

2.1 Data model

Consider a uniform linear array (ULA) with M sensors and P narrowband far-field signal source impinging on the ULA from angular direction θ_p, which space half of the wavelength. The sensor received signal kth sample can be modeled as

$$X(k) = \sum_{p=1}^{P} AS_k(\theta_p) + N(k) \tag{1}$$

where **X(k)** is the array received observation vector

$$X(k) = [X_1(k), X_2(k), \cdots, X_M(k)]^T \in C^{M\times N} \tag{2}$$

$\mathbf{A_m}$ is an ideal steering matrix when setting the first sensor as the reference

$$A = \left[1, e^{-j\pi \sin(\theta_p)}, \cdots, e^{-j(M-1)\pi \sin(\theta_p)}\right]^T \in C^{M\times P} \tag{3}$$

$\mathbf{S_k(\theta)}$ is the signal vector

$$S_k(\theta) = [S_k(\theta_1), S_k(\theta_2), \cdots, S_k(\theta_P)]^T \tag{4}$$

N(k) is alpha-stable noise

$$N(K) = [N_1(k), N_2(k), \cdots, N_M(k)]^T \tag{5}$$

Our objective is to estimate the DOA (θ_1, θ_2, ..., θ_p) of the source from **X(k)**, the second-order statistical is the most commonly used method, that is

$$R = E\left[XX^H\right] \tag{6}$$

In practice, the covariance matrix **R** can be estimated with a finite number of snapshots via

$$\hat{R} = \frac{1}{N}\sum_{k=1}^{N} X(k)X^H(k) \in C^{M\times M} \tag{7}$$

By performing eigenvalue decomposition (EVD) on $\mathbf{R}^{\wedge}$, we can obtain

$$\hat{R} = U\Lambda U^H = U_S\Lambda_S U_S^H + U_n\Lambda_n U_n^H \tag{8}$$

where $\mathbf{U} = [\mathbf{U_s}, \mathbf{U_n}]$, $\mathbf{U_s}$, and $\mathbf{U_n}$ are the noise and signal subspace matrices and $\mathbf{\Lambda_s}$ and $\mathbf{\Lambda_n}$ are the corresponding eigenvalue matrices. According to the orthogonality between noise and signal subspaces [21], $\mathbf{U_s} \perp \mathbf{U_n}$, spatial power spectrum can be obtained from

$$P_{MUSIC} = \frac{1}{a^H(\theta)U_n U^H{}_n a(\theta)} \quad -90^\circ \le \theta \le 90^\circ \tag{9}$$

2.2 Alpha-stable noise (*SaS*)

Recent studies show that alpha-stable distribution is well suited for describing impulsive noise [12], which is defined by a characteristic function

$$\phi(t) = \exp(j\xi t - \gamma|t|^\alpha[1 + j\beta sign(t)\omega(t,\alpha)]) \tag{10}$$

where

$$\omega(t,\alpha) = \begin{cases} \tan\left(\frac{\alpha\pi}{2}\right), & \alpha \neq 1 \\ \frac{\pi}{2}\log|t|, & \alpha = 1 \end{cases} \tag{11}$$

$$signt(t) = \begin{cases} 1, & t > 0 \\ 0, & t = 0 \\ -1, & t < 0 \end{cases} \tag{12}$$

As can be seen from the above Eqs. (10, 11 and 12), alpha-stable distribution is determined by α, β, γ, and μ, and its characteristics are as follows.

(1) α is the characteristic exponent which is characterized the strength of the impulsiveness, the smaller α, the heavier the tails of the alpha-stable probability density function, $0 < \alpha \le 2$;
(2) β is the symmetry parameter which is characterized by the level of out-of-center for alpha-stable probability density function. Alpha-stable distribution is called symmetric alpha stable ($S\alpha S$) when $\beta = 0$, $-1 \le \beta \le 1$;
(3) γ is the dispersion parameter which is characterized by the degree of out-of-mean for the random variable, $\gamma > 0$;
(4) ξ is the location parameter which is determined by the central position of alpha-stable distribution. ξ denotes the mean of the random variable when the α satisfies with $1 < \alpha \le 2$; ξ denotes the median of the random variable when the characteristic exponent satisfies $0 < \alpha < 1$, $-\infty < \xi < +\infty$.

Figure 1 presents the symmetric α-stable probability density functions, and Figs. 2 and 3 are the $S\alpha S$ distributed signal in the time domain. There are some especial distributions as follows: Gaussian ($\alpha = 2$, $\beta = 0$, $\gamma = 1$, $\xi = 0$), Cauchy ($\alpha = 1$, $\beta = 0$, $\gamma = 1$, $\xi = 0$), Levy ($\alpha = 0.5$, $\beta = -1$, $\gamma = 1$, $\xi = 0$). The Matlab code was used to generate a complex isotropic symmetric alpha-stable distribution reference as ROC-MUSIC [13].

3 Proposed solution

In this section, we proposed a new operator correntropy-based covariance matrix (CBCM), and it applied with MUSIC to estimating DOA in the presence of an impulsive noise environment. We present the definition of correntropy in Section 3.1 and correntropy-induced metric (CIM) in Section 3.2. Correntropy-based

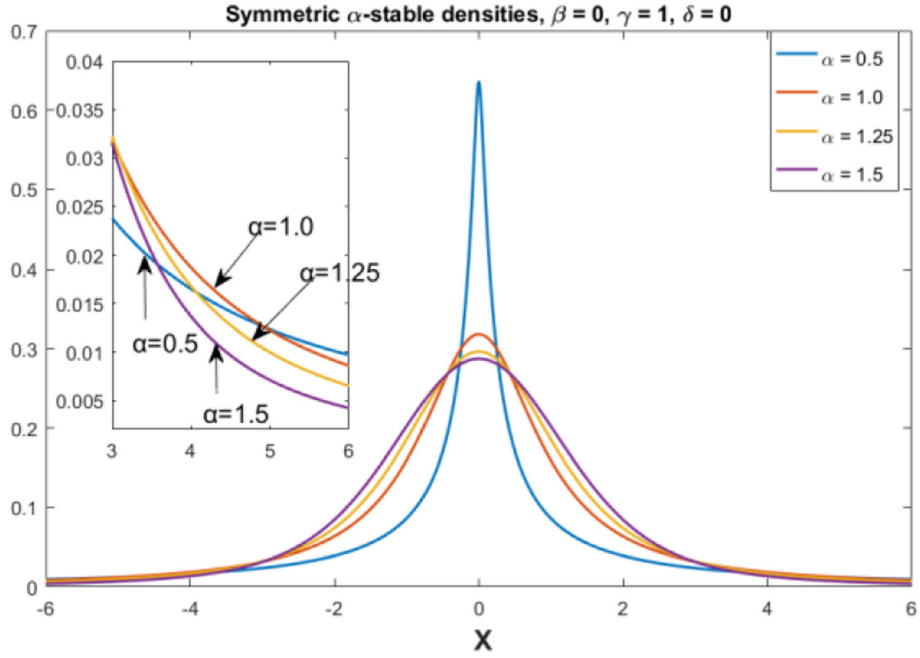

Fig. 1 Symmetric α-stable probability density functions with different α ($\beta = 0$, $\gamma = 1$, $\xi = 0$)

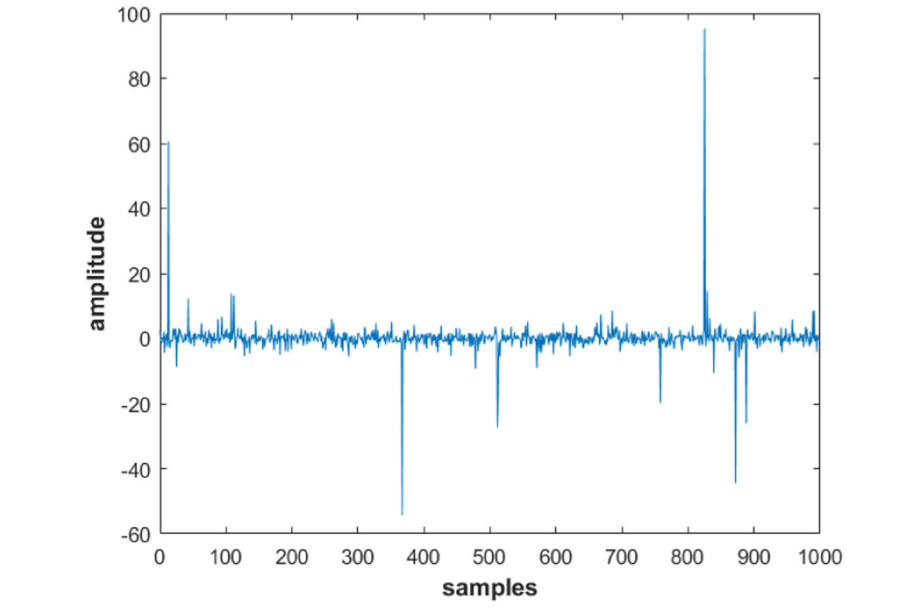

Fig. 2 *SaS* distributed signal with $\alpha = 1.5$

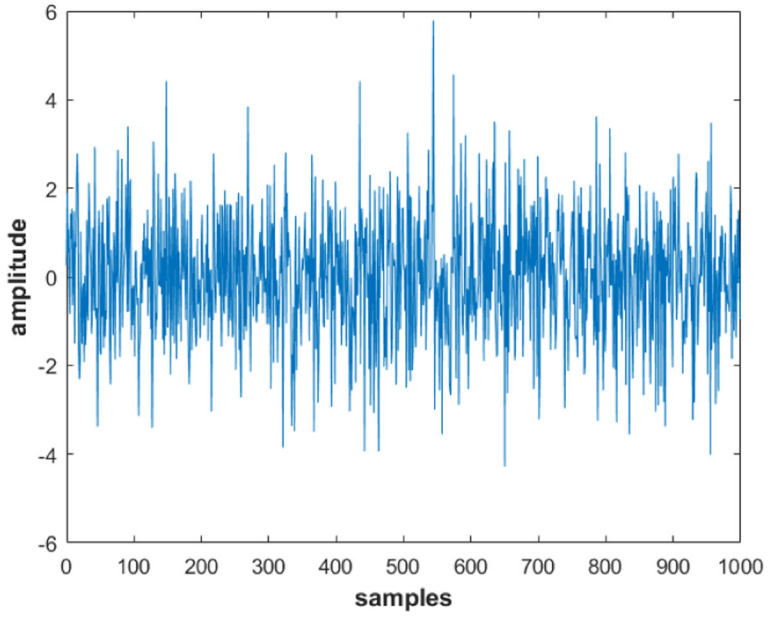

Fig. 3 *SaS* distributed signal with $a = 2$

covariance matrix was proposed in Section 3.3, and then the implementation of CBCM-MUSIC algorithm is given.

3.1 Correntropy

For two arbitrary random variables **X** and **Y**, the cross correntropy defined by [17]:

$$V_\sigma(X, Y) = E[\kappa_\sigma(X - Y)] \tag{13}$$

where $\kappa_\sigma(\bullet)$ is the kernel function that satisfies Mercer's theory, σ is the kernel size, and $E[\bullet]$ represents the mathematical expectation. In practice, the joint probability density function (pdf) is unknown, and only a finite number of data $\{[x_i, y_i]^N_{i=1}\}$ can obtain to estimate the correntropy for random variables **X** and **Y**,

$$\hat{V}_\sigma(X, Y) = \frac{1}{N}\sum_{i=1}^{N}\kappa_\sigma(x_i - y_i) \tag{14}$$

In general, we use the Gaussian kernel $k_\sigma(\bullet)$, using Taylor series expansion for Eq. (14), and the correntropy can be rewritten as [17]

$$k_\sigma(\cdot) = \frac{1}{\sqrt{2\pi}\sigma}\exp\left(-\frac{(\cdot)^2}{2\sigma^2}\right) \tag{15}$$

$$V_\sigma(X, Y) = \frac{1}{\sqrt{2\pi}\sigma}\sum_{n=0}^{\infty}\frac{(-1)^n}{2^n n!}E\left[\frac{(X-Y)^{2n}}{\sigma^{2n}}\right] \tag{16}$$

Equation (16) indicates that correntropy involves all the even-order moments of the (***X-Y***); note that if $n = 1$, we can get

$$E\left[(X-Y)^2\right] = E\left[X^2\right] + E\left[Y^2\right] - 2E[XY] \tag{17}$$

Equation (17) reveals that correntropy includes the conventional relation.

3.2 Correntropy-induced metric

Correntropy can also induce a metric (CIM) [18]. There are two vector $\boldsymbol{a} = (a_1, a_2, \cdots, a_N)^T$ and $\boldsymbol{b} = (b_1, b_2, \cdots, b_N)^T$, and the function CIM defines as

$$CIM(a,b) = (\kappa_\sigma(0) - V(a,b))^{0.5} \tag{18}$$

Apparently, when the Gaussian kernel is used,

$$\kappa_\sigma(0) = \frac{1}{\sqrt{2\pi}\sigma} \tag{19}$$

The properties of CIM can be listed as follows:

(1) Nonnegativity:

$\mathrm{CIM}(\boldsymbol{a},\boldsymbol{b}) \geq 0$, $\mathrm{CIM}(\boldsymbol{a},\boldsymbol{b}) = 0$ if and only if $\boldsymbol{a} = \boldsymbol{b}$;

(2) Symmetric:

$\mathrm{CIM}(\boldsymbol{a},\boldsymbol{b}) = \mathrm{CIM}(\boldsymbol{b},\boldsymbol{a})$;

(3) Triangle inequality:

$\mathrm{CIM}(\boldsymbol{a},\boldsymbol{c}) \leq \mathrm{CIM}(\boldsymbol{a},\boldsymbol{b}) + \mathrm{CIM}(\boldsymbol{b},\boldsymbol{c})$.

Figure 4 shows the contours of distance from X to the origin in a 2D space, and Fig. 5 displays the surface. Compared with the conventional metric, CIM presents "mix norm" property. From Fig. 4, we can see that three zones have been divided. This metric divides space into three regions named the Euclidean region, transition region, and rectification

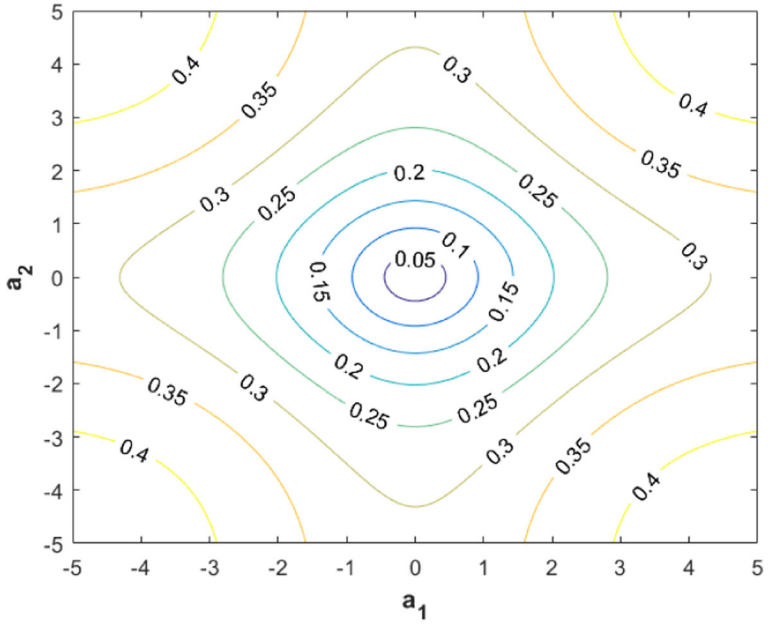

Fig. 4 The contours of CIM $\sigma = 2$

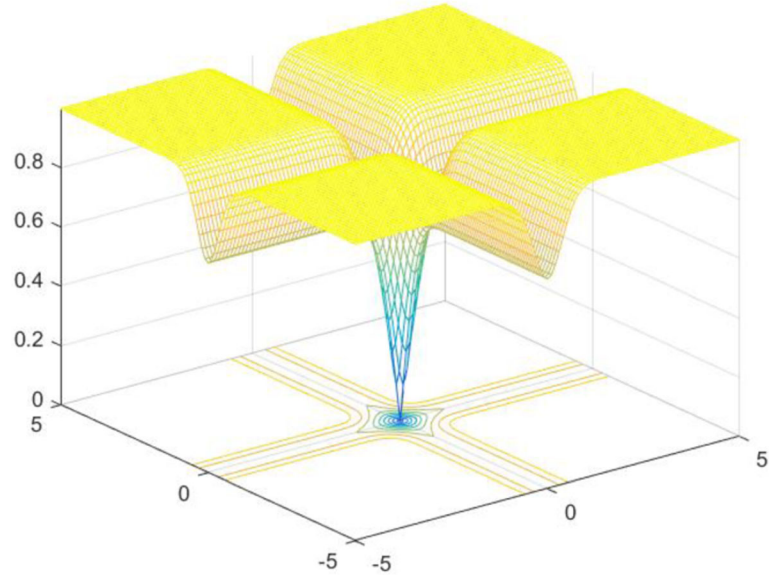

Fig. 5 CIM surface plot showing to distant regions $\sigma = 0.4$

region [18]. In the Euclidean region, CIM behaves as l_2-norm, in the transition region, CIM behaves as l_1-norm, and in rectification region, CIM behaves like l_0-norm. The kernel size σ controls the bandwidth of the CIM "mix norm."

3.3 Correntropy-based covariance matrix

Theorem 1 If $\boldsymbol{X}$ and $\boldsymbol{Y}$ are jointly $S\alpha S$ and have a symmetric distribution, the correntropy-based covariance matrix by using the Gaussian kernel of $\boldsymbol{X}$ and $\boldsymbol{Y}$ can be defined as

$$R_{CBCM} \triangleq E\left[\exp\left(-\frac{(X-\mu Y)^2+(Y-\mu X)^2}{2\sigma^2}\right)XY\right] \quad 0<\mu<1 \tag{20}$$

where μ is the suppression parameter and σ is the kernel size.

The proof of the boundedness of CBCM reference as Appendix B [16], here, inspired by the phase fractional lower-order moment; the suppression parameter μ is introduced to exert different suppressed effects on random variables $\boldsymbol{X}$ and $\boldsymbol{Y}$. Equation (21) can be expressed as

$$R_{CBCM} \triangleq E\left[\exp\left(-\frac{(X-\mu Y)^2}{2\sigma^2}\right)X\exp\left(-\frac{(Y-\mu X)^2}{2\sigma^2}\right)Y\right] \quad 0<\mu<1 \tag{21}$$

3.4 The implementation of CBCM-MUSIC

Summarizing the existing algorithms, knowing that the key to implementing DOA is to modify the conventional covariance matrix to suit for impulsive noise environment, then the DOA estimation can be implemented in combination with the subspace technology. Inspired by correntropy and Gaussian kernel function to suppress impulse noise, and the prior parameters of noise do not need to know, this paper proposed a

modified covariance matrix (CBCM) based on correntropy with Gaussian kernel function.

CBCM cannot only preserve the similarity measure in the sense for two random variables, but also it can suppress the "outliers" by using the rapid reduction of the exponential function; thus, CBCM achieves the purpose of adapting to the environment.

The main steps of the CBCM-MUSIC are summarized as follows:

Step 1. Compute the $M \times M$ matrix $\hat{\mathbf{R}}$, whose (i,j)th entry is

$$\mathrm{R}_{\mathrm{i,j}} = \frac{1}{\mathrm{N}}\sum_{\mathrm{n}=1}^{\mathrm{N}}\left[\exp\left(-\frac{\left(\mathrm{x_i(n)}\text{-}\mu\mathrm{x_j(n)}\right)^2 + \left(\mathrm{x_j(n)}\text{-}\mu\mathrm{x_i(n)}\right)^2}{2\sigma^2}\right)\mathrm{x_i(n)x_j^*(n)}\right] \quad 0 < \mu < 1 \tag{22}$$

Section 4.1 gives the discussion for the selection of the suppression parameter μ and kernel size σ.

Step 2. Perform eigenvalue decomposition (EVD) on the covariance matrix $\hat{\mathbf{R}}$ to obtain the noise subspace matrix $\hat{\mathbf{U}}_{\mathbf{n}}$

Step 3. Compute the corresponding CBCM-MUSIC spatial spectrum via

$$P_{CMCB-MUSIC} = \frac{1}{a^H(\theta)U_N U^H{}_N a(\theta)} \qquad -90^\circ \le \theta \le 90^\circ \tag{23}$$

Step 4. Choose P local peaks of $\mathbf{P}_{\mathrm{CMCB\text{-}MUSIC}}$ as the estimates of DOAs.

4 Simulation and results

To assess the performance of the CBCM-MUSIC, two performance criteria are used to evaluate the proposed algorithms: the probability of resolution and RMSE (root-mean-square-error). The two sources are recognized to be successfully resolved if and only if [6]

$$\frac{f(\theta_1)+f(\theta_2)}{2} > f\left(\frac{\theta_1+\theta_2}{2}\right) \tag{24}$$

where $f(\cdot)$ stands for the spectral value. Root-mean-square-error (RMSE) can be expressed as

$$RMSE = \sqrt{\frac{1}{400}\sum_{i=1}^{200}\sum_{p=1}^{2}\left(\hat{\theta}_{i,p} - \theta_p\right)^2} \tag{25}$$

where θ_p is the actual angle of the pth signal, and $\hat{\theta}_{i,p}$ is the estimated angle of θ_p in the ith Monte-Carlo trial, where $i = 1, 2, \cdots, 200$. All the numerical results were obtained with 200 independent trials.

In the following experiments, this paper considers two sources (Gaussian, QPSK, BPSK, QAM, PAM) that have the same variance imping on a uniform linear array (ULA), an $M = 8$ elements ULA with an interelement spacing equal to half a wavelength, supposing that the source number is known. A generalized signal-to-noise (GSNR) ratio was used to describe signal-to-noise ratio [13], that is

$$GSNR = 10\ \lg\left(\frac{\sigma_S^2}{\gamma}\right) \tag{26}$$

$$\hat{\sigma}_S^2 = \frac{1}{N}\sum_{n=1}^{N}\left|\hat{\sigma}_s^2(n)\right|^2 \tag{27}$$

where N indicates the snapshots, γ indicates the dispersion parameter, and $\sigma^2{}_s$ indicates the signal power.

Section 4.1 gives the recommendations for the selection of parameters; Section 4.2 compares the DOA spatial spectrum for ROC-MUSIC, FLOM-MUSIC, PFLOM-MUSIC, CRCO-MUSIC, and CBCM-MUSIC; finally, the performance of analysis for CBCM-MUSIC presents in Section 4.3.

4.1 Parameter selection

In this section, we have discussed the selection of the parameters of the CBCM-MUSIC algorithm, including the kernel size σ and suppression parameter μ. According to the correntropy, the kernel bandwidth σ is full and controls the scale of the CIM norm, that is, a small kernel size will lead to a tight linear region (L_2 norm) and to a large L_0 region. The selection of the kernel size is described as conventional signals that fall into L_2 norms and impulse signals that fall into L_1 and L_2 norms.

In order to make kernel size σ and suppression parameter μ widely applicable, different types of communication signals were used to DOA's sources embedded in complex isotropic $S\alpha S$ noise, such as quaternary amplitude modulation (QAM), binary phase-shift keying (BPSK), quaternary phase-shift keying (QPSK), and Gaussian source, note that BPSK is noncircular signals.

4.2 Suppression parameter μ

Suppression parameter μ is limited in the range of [0, 1], and the covariance matrix degenerates into a traditional covariance matrix when $\mu = 1$. Snapshots $N = 256$, a moderate impulsive noise condition with $\alpha = 1.4$, GSNR = 8 dB, ULA with 8 sensors, we select the kernel size $\sigma = 8$ tentatively.

Figure 6 illustrates the influence of the suppression parameter, we can see that $\mu \in [0.5, 0.9]$ would be the optimal fields for CBCM-MUSIC, and the suppression parameter μ is relatively small over a wide range of $\mu \in [0.4, 0.9]$ to Monte-Carlo runs in terms of RMSE of CBCM-MUSIC. According to Figs. 6 and 7, the desired results are achieved at $\mu = 0.7$; hence, in the following experiment, we perform Monte-Carlo runs with $\mu = 0.7$.

4.2.1 Kernel size σ

Snapshots $N = 256$, $\mu = 0.7$, and GSNR = 8 dB. $\alpha = 1.4$, ULA with 8 sensors. From Figs. 8 and 9, it can be seen that the CBCM-MUSIC algorithm obtains better DOA

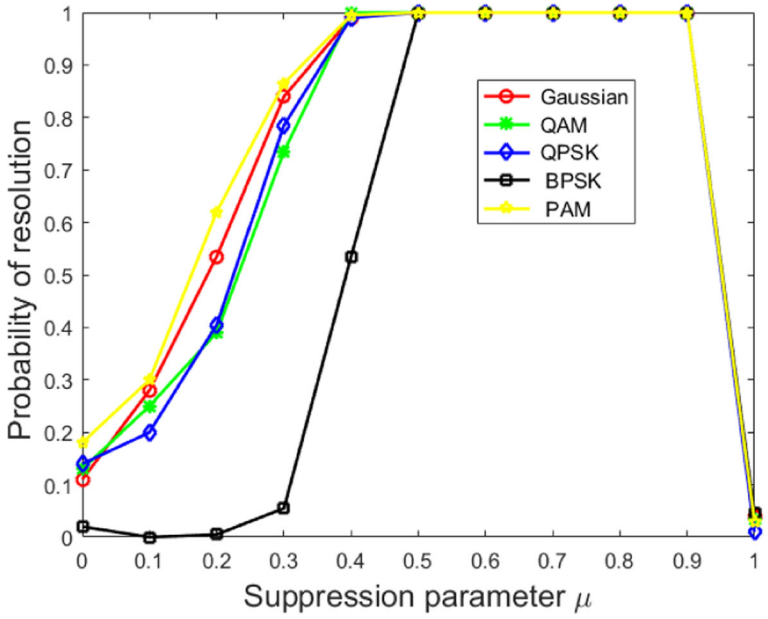

Fig. 6 Probability of resolution against suppression parameter μ

estimation performance in the range of $\sigma \in [6, 20]$, but the optimal value of the kernel size cannot be determined.

Since the selection of σ is closely related to GSNR [16], the rectification region is affected by the kernel size. Below, the RMSE and probability of resolution are analyzed at different GSNR $\sigma \in [2, 20]$, $\mu = 0.7$, and $\alpha = 1.4$. From Figs. 10 and 11, we can observe that kernel size $\sigma = 10$ would be the optimal value for CBCM-MUSIC to reach its best performance. In particular, the probability of resolution in low SNR and high impulsive environments is shown in Fig. 10. Based on the above description and discussion, the

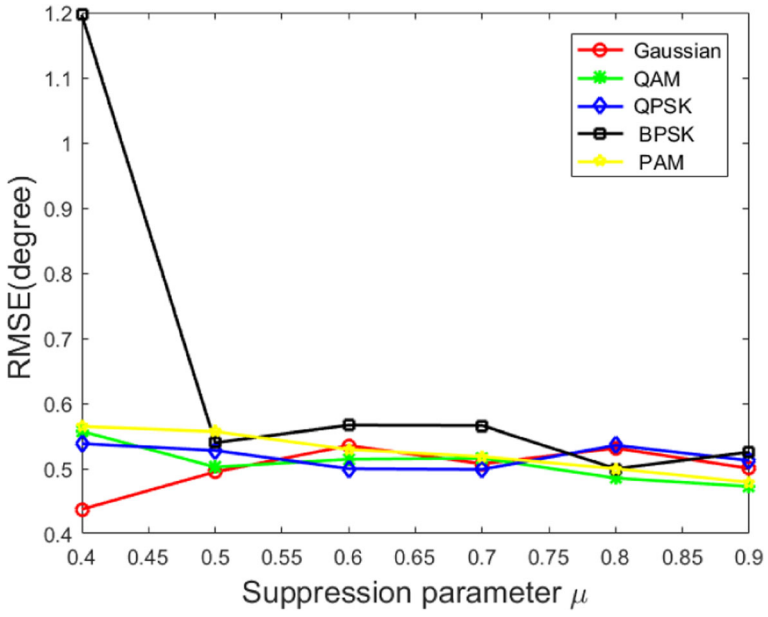

Fig. 7 RMSE against suppression parameter μ

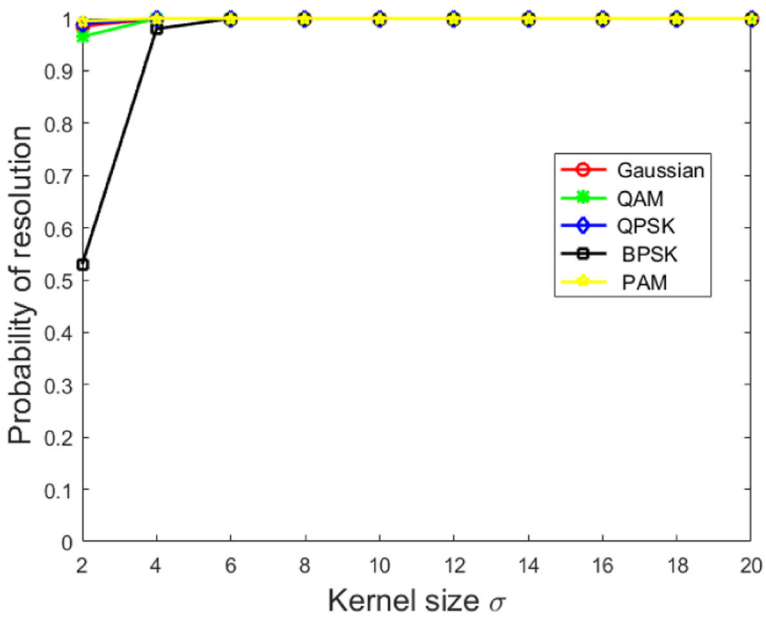

Fig. 8 Probability of resolution against kernel size σ

simulations in Section 4.2 and Section 4.3 are implemented by setting $\mu = 0.7$ and $\sigma = 10$.

4.3 Spatial spectrum estimation

In order to directly show the performance of the proposed CBCM-MUSIC algorithm, we also compare spatial spectrum with that of the ROC-MUSIC ($p = 1.1$) [13], FLOM-MUSIC ($p = 1.1$) [14], PFLOM-MUSIC ($p = 0.2$) [15], and CRCO-MUSIC ($\mu = 0.5$, $\sigma =$

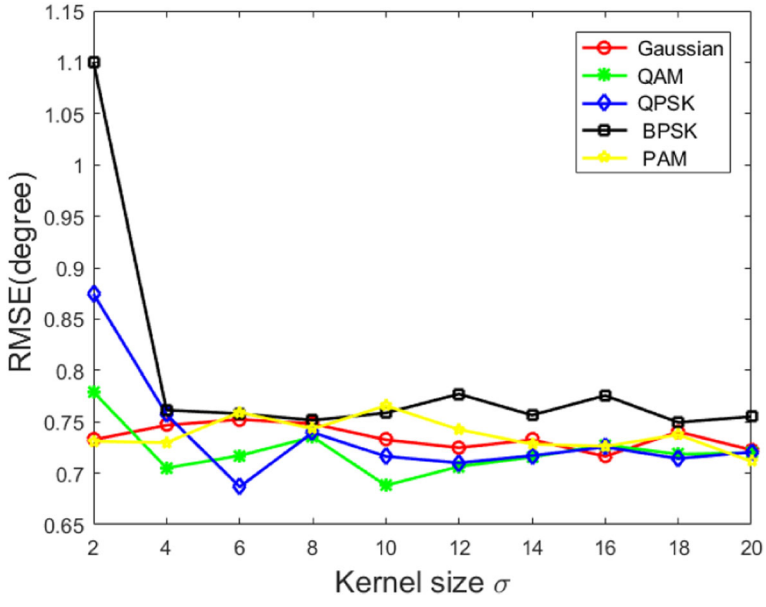

Fig. 9 RMSE against kernel size σ

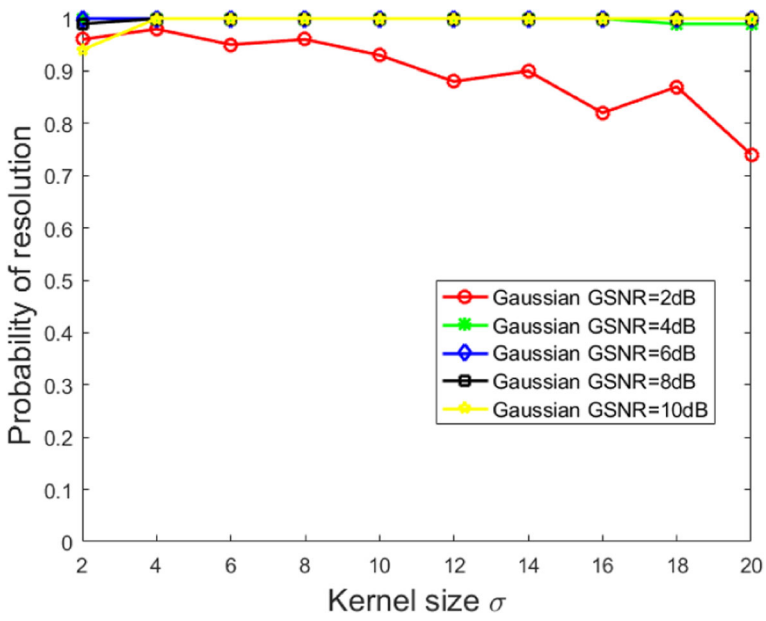

Fig. 10 Probability of resolution against kernel size σ under different GSNR

1.4sqrt($\sigma_s^{\wedge 2}$)) [16], where $\sigma_s^{\wedge 2}$ is the estimated variance of the noise-free signal **S** and p is the order of the moment. Consider a uniform linear array of 8 sensors with an inter-spacing of half a wave is used, two uncorrelated Gaussian sources ($\theta_1 = -5°$, $\theta_2 = 5°$) impinge on this array, GSNR = 8 dB, snapshots $N = 256$, and $\alpha = 1.4$.

The results of 10 runs of the normalized spatial spectrum are displayed in Fig. 12. Comparing the results of the above five algorithms, we can observe that CBCM-MUSIC algorithm shows better focus ability for true DOA under impulsive noise environments, the performance of MUSIC is degraded seriously and 10 runs fail to

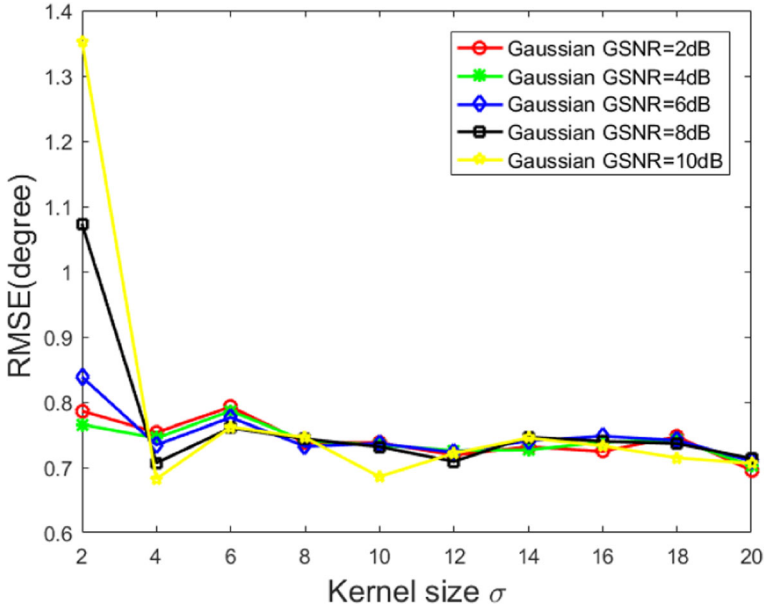

Fig. 11 RMSE against kernel size σ under different GSNR

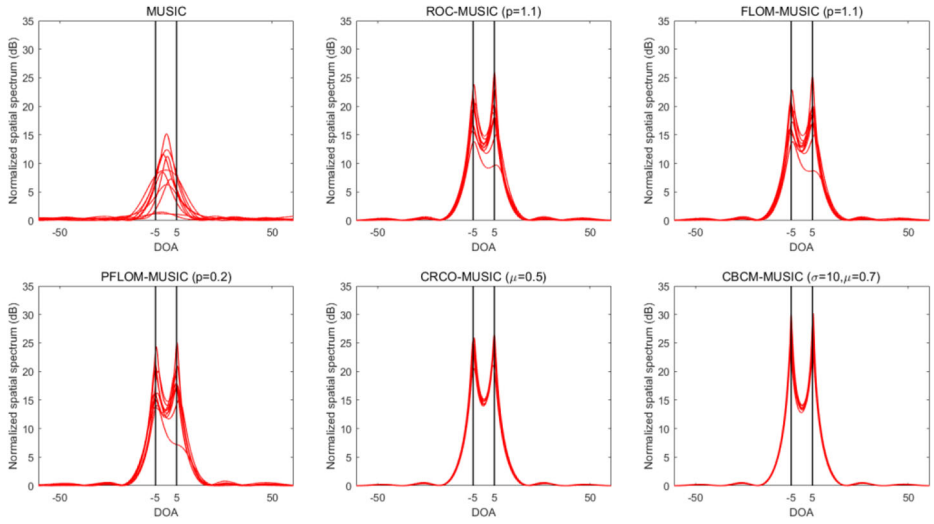

Fig. 12 The normalized spatial spectrum of the algorithms (black lines: true DOAs)

distinguish two incident signals successfully. Seeing the performance degradation of the MUSIC, ROC-MUSIC, FLOM-MUSIC, and PFLOM-MUSIC algorithms in the impulsive noise environment by no means, further analyses are made in the following experiments.

4.4 Performance analysis

In this section, the performance of the proposed CBCM-MUSIC algorithm is compared with CRCO-MUSIC (μ = 0.5, σ = 1.4sqrt($\sigma_s^{\wedge 2}$)) [16] and SCM-MUSIC [22]. In terms of resolution probability and RMSE, the performance of the number of snapshots, GSNR, characteristic exponent α, and angular separation is investigated in this experiment.

4.4.1 Effect of the number of snapshots

In the first experiment, we study the effect of the number of snapshots and the results are exhibited in Figs. 13 and 14. An M = 8 element ULA with an interspacing of half a wave is used, two independent QAM sources are located at θ_1 = − 5° and θ_2 = 5°, the complex isotropic SαS is α = 1.4, and the GSNR is set as a constant at 8 dB. From Fig. 13, we can observe that CBCM–MUSIC gains a more evident decrease in RMSE than the other algorithms as the number of the snapshots increases. Figure 14 displays the probability of resolution against snapshots.

4.4.2 Effect of the GSNR

Figures 15 and 16 illustrate the performance of CBCM-MUSIC, CRCO-MUSIC [16], and SCM-MUSIC [22] under a wide range of GSNRs from 0 to 10 dB, and the number of snapshots available to the algorithms is N = 256. A moderate impulsive noise α = 1.4 embedded in two QAM sources (θ_1 = − 5°, θ_2 = 5°). Figures 15 and 16 depict the improved performance of CBCM-MUSIC over that conventional algorithm both in terms of resolution probability and RMSE.

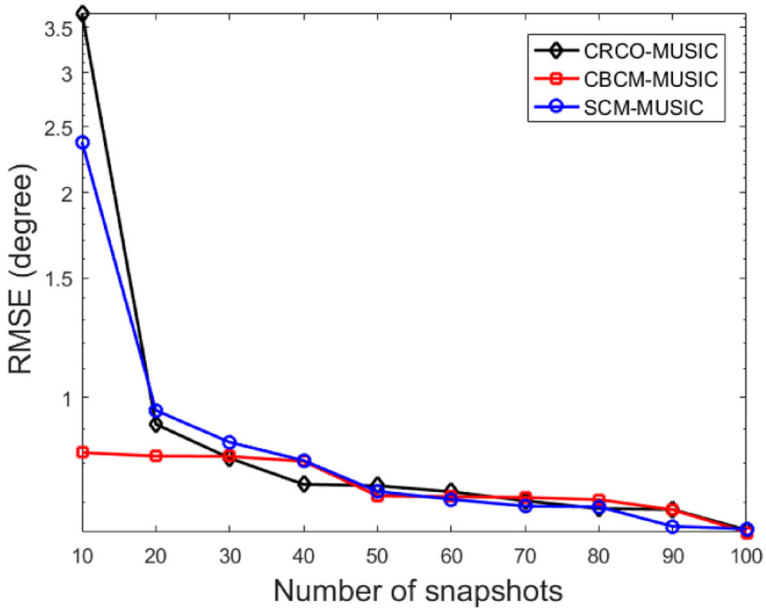

Fig. 13 RMSE against snapshots

4.4.3 Effect of the characteristic exponent α

In this experiment, we study the robustness of the CBCM-MUSIC algorithm under a wide range of characteristic exponent α from 0.6 to 2. Consider two QAM sources ($\theta_1 = -5°$, $\theta_2 = 5°$) impinge on the ULA with 8 sensors, the GSNR = 8 dB and the number of snapshots N = 256. Fig. 17 and Fig. 18 give the simulation results. We note that CBCM-MUSIC showed better performance than SCM-MUSIC and CRCO-MUSIC as the characteristic exponent α is decreased.

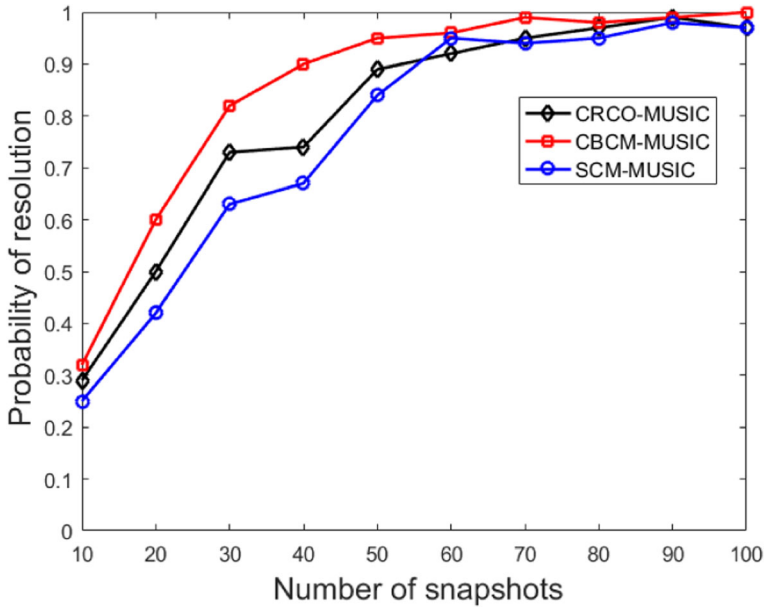

Fig. 14 Probability of resolution against snapshots

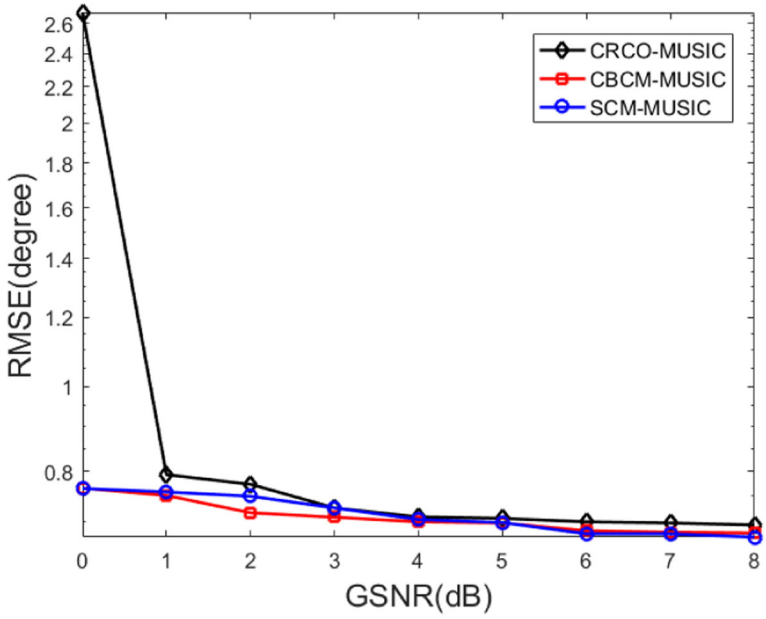

Fig. 15 RMSE against GSNR

4.4.4 Effect of the angular separation

In the final experiment, we study the variation of the algorithmic performance with respect to the angular separation of the two incoming QAM signals, for $N = 256$, GSNR = 10 dB, and $\alpha = 1.4$. As expected, by contrast with the performance of the SCM-MUSIC and CRCO-MUSIC, the resolution capability of CBCM-MUSIC algorithms is improved with increasing angle-separated value between the two sources based on Figs. 19 and 20.

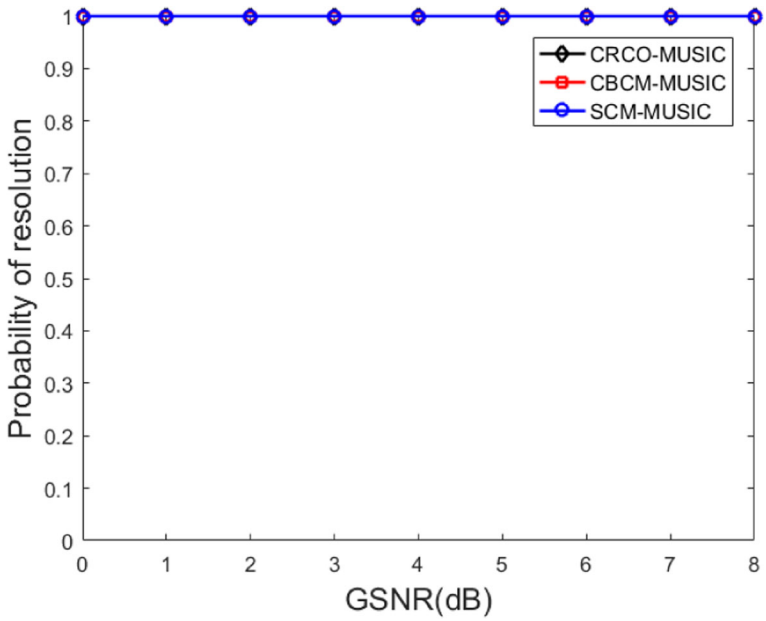

Fig. 16 Probability of resolution against GSNR

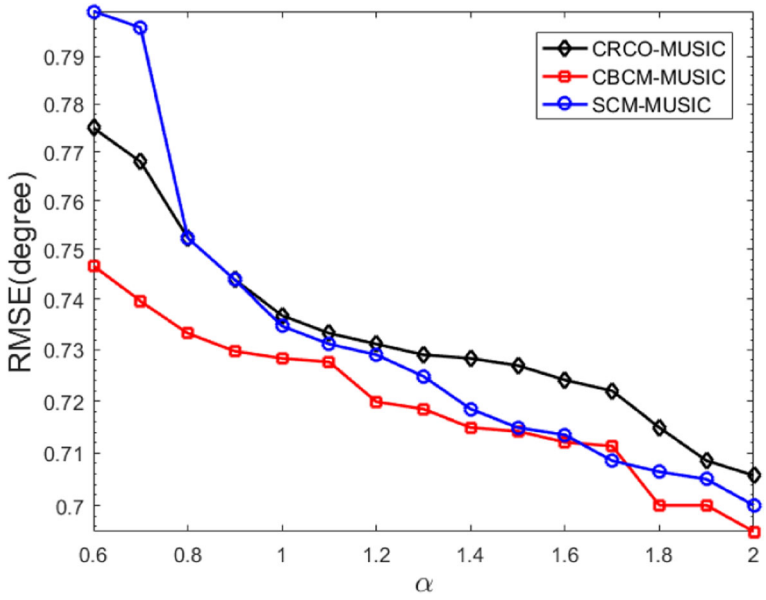

Fig. 17 RMSE against characteristic exponent α

5 Discussion

In this paper, we proposed a novel method that formulated the covariation matrix of the sensor outputs under the impulsive noises, which is based on correntropy. The improved performance of the proposed CBCM-MUSIC algorithm in the presence of a wide range of impulsive noise environments was demonstrated via Monte-Carlo experiments.

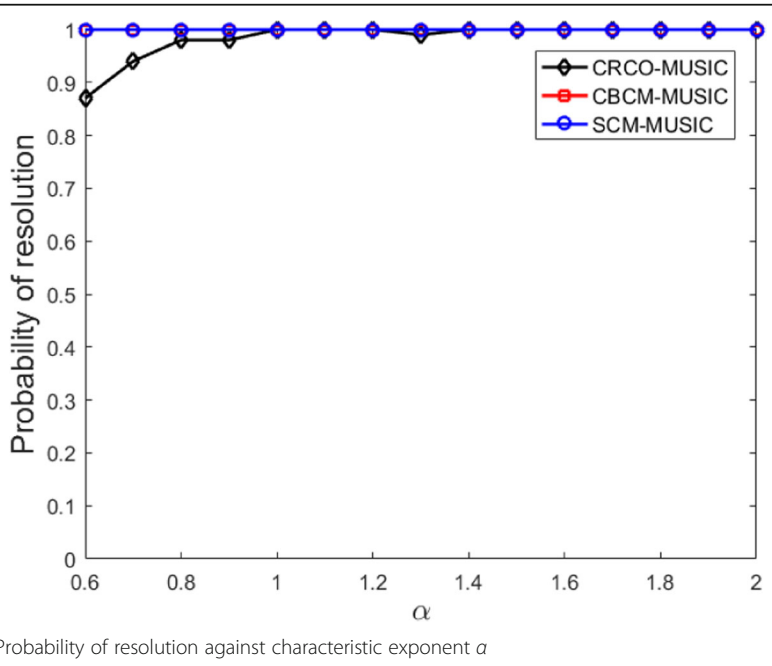

Fig. 18 Probability of resolution against characteristic exponent *α*

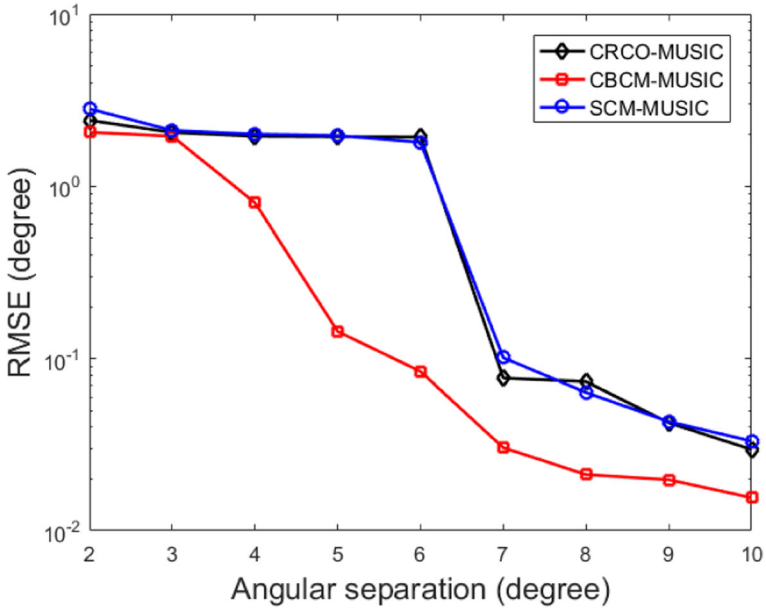

Fig. 19 RMSE against the angular separation

This paper assumed sources are independent that illuminated the array sensor. In many practical conditions, the sources are coherent signals due to multipath; hence, future research includes the development of methods for the DOA of the coherent signals in the presence of impulsive noise. Secondly, we will address the problem of localizing multiple wide-band sources in impulsive noise

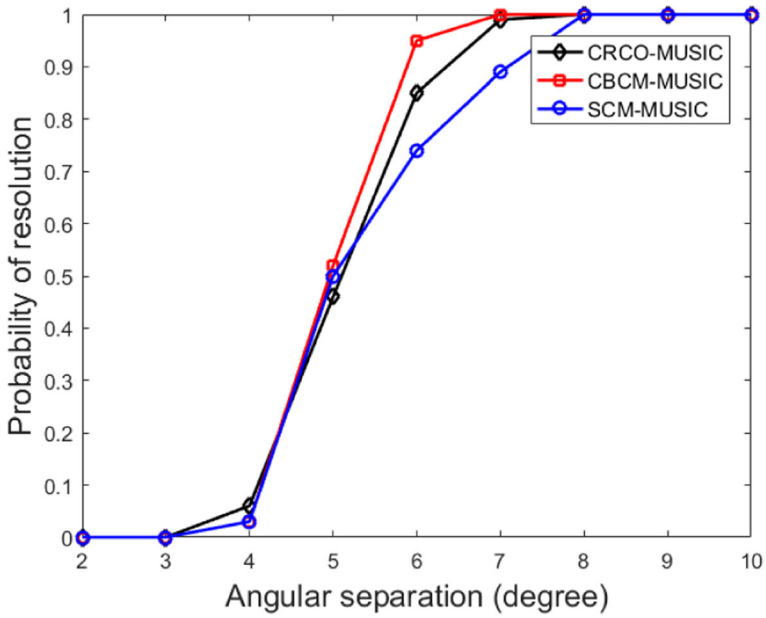

Fig. 20 Probability of resolution against the angular separation

Abbreviations
BPSK: Binary phase-shift keying; CBCM: Correntropy-based covariance matrix; CIM: Correntropy-induced metric; CRCO: Correntropy-based correlation; DOA: Direction of arrival; EVD: Eigenvalue decomposition; FLOM: Fractional lower-order moments; FLOS: Fractional lower-order statistic; GSNR: Generalization signal to noise ratio; MUSIC: Multiple signal classification; pdf: Probability density function; PFLOM: Phase-FLOM; QAM: Quaternary amplitude modulation; QPSK: Quaternary phase-shift keying; ROC-MUSIC: Robust covariance-MUSIC; *SaS*: Symmetric alpha stable; ULA: Uniform linear array

Acknowledgements
This work has been supported by the National Natural Science Foundation of China (Grant No: 61701344), Tianjin Higher Education Creative Team Funds Program in China, and Tianjin Normal University Doctoral Foundation (52XB1603, 52XB1713). I sincerely thank the anonymous referees for their technical suggestions and their advice on decorum.

Authors' contributions
JinChen gives the overall research direction and ideas. ShengGuan read the relevant literature and books and drafts the article and makes the corresponding experimental simulation. The author(s) read and approved the final manuscript.

Authors' information
Jin Chen was born in Wuhu, China, in 1976. He received the M.S. degree from Tianjin Normal University and the Ph.D. degree from College of Precision Instrument and Opto-electronics Engineering, Tianjin University, in 2002 and 2013, respectively. Since 2005, he has been working at Tianjin Normal University. He is an associate professor of the Tianjin Key Laboratory of Wireless Mobile Communications and Power Transmission. His research interests include acoustic signal acquisition and processing, broadband sensor array signal processing, and artificial intelligence.
Sheng Guan was born in JiLin, China, in 1993. He received the B.S. degree in textile engineering from the Inner Mongolia University of Technology in 2017. He is currently working toward the M.S. degree in information and communication engineering at Tianjin Normal University. His research interests include beamforming optimization and nonstationary signal processing.

Availability of data and materials
Not applicable.

Competing interests
The authors declare that they have no competing interests.

Received: 11 September 2019 Accepted: 14 July 2020
Published online: 28 July 2020

References
1. A. Hassanien, S.A. Vorobyov, Phased-MIMO radar: A tradeoff between phased-array and MIMO radars. IEEE Trans Signal Processing **58**(6), 3137–3151 (2010)
2. J.J. Jiang, F.J. Duan, X.Q. Wang, A universal two-dimensional direction of arrival estimation method without parameter match. IEEE Sensors J. **16**(9), 3141–3146 (2016)
3. S.T. Yuan, Q.L. Liang, 3D nested distributed massive MIMO: Modeling and performance analysis. Ad Hoc Netw. **58**, 6–12 (2016)
4. H. Yin, D. Gesbert, M. Filippou, Y. Liu, A coordinated approach to channel estimation in large-scale multiple-antenna systems. IEEE J Selected Areas Commun **31**(2), 264–273 (2013)
5. A.F. Molisch et al., Hybrid beamforming for massive MIMO: A survey. IEEE Commun. Mag. **55**(9), 134–141 (2017)
6. N. Wu, F.Q. Zhu, Q.L. Liang, Evaluating spatial resolution and channel capacity of sparse cylindrical arrays for massive MIMO. IEEE Access **5**, 23994–24003 (2017)
7. M. Carlin, P. Rocca, G. Oliveri, F. Viani, A. Massa, Directions-of-arrival estimation through Bayesian compressive sensing strategies. IEEE Trans Antennas Propagation **61**(7), 3828–3838 (2013)
8. M.D. Button, J.G. Gardiner, I.A. Glover, Measurement of the impulsive noise environment for satellite-mobile radio systems at 1.5 GHz. IEEE Trans Vehicular Technol **51**(3), 551–560 (2002)
9. K.L. Blackard, T.S. Rappaport, C.W. Bostian, Measurements and models of radio frequency impulsive noise for indoor wireless communications. IEEE J Selected Areas Commun **11**(7), 991–1001 (1993)
10. A. Chandraa, Measurements of radio impulsive noise from various sources in an indoor environment at 900 MHz and 1800 MHz, 13th IEEE International Symposium on Personal, Indoor and Mobile Radio Communications, Lisboa, Portugal, 639-643 (2002).
11. B. Stuck, B.A. Kleiner, Statistical analysis of telephone noise. Bell System Tech J **53**(7), 1263–1320 (1974)
12. C.L. Nikias, M. Shao, *Signal Processing with α-Stable Distribution and Applications* (Wiley, New York, 1995)
13. P. Tsakalides, C.L. Nikias, Robust covariation-based MUSIC (ROC-MUSIC) algorithm for bearing estimation in impulsive noise environments. IEEE Trans. Signal Process. **44**(7), 1623–1633 (1996)
14. T.H. Liu, J.M. Mendel, A subspace-based direction finding algorithm using fractional lower order statistics. IEEE Trans. Signal Process. **49**(8), 1605–1613 (2001)
15. H. Belkacemi, S. Marcos, Robust subspace-based algorithms for joint angle/Doppler estimation in non-Gaussian clutter. Signal Process. **87**(7), 1547–1558 (2007)
16. J. Zhang, T. Qiu, A. Song, H. Tang, A novel correntropy based DOA estimation algorithm in impulsive noise environments. Signal Process. **104**, 346–357 (2014)

17. I. Santamaría, P.P. Pokharel, J.C. Principe, Generalized correlation function: Definition, properties and application to blind equalization. IEEE Trans. Signal Process. **54**(6), 2187–2197 (2006)
18. W. Liu, P.P. Pokharel, J.C. Príncipe, Correntropy: Properties and applications in non-Gaussian signal processing. IEEE Trans Signal Proc **55**(11), 5286–5298 (2007)
19. A. Song, T. Qiu, The equivalency of minimum error entropy criterion and minimum dispersion criterion for symmetric stable signal processing. IEEE Signal Proc Lett **17**(1), 32–35 (2010)
20. R. He, W.S. Zheng, B.G. Hu, Maximum correntropy criterion for robust face recognition. IEEE Trans Pattern Anal Machine Intell **33**(8), 1561–1576 (2011)
21. R.O. Schmidt, Multiple emitter location and signal parameter estimation. IEEE Trans. Antennas and Propagation **34**(3), 276–280 (1986)
22. S. Visuri, H. Oja, V. Koivunen, Subspace-based direction-of-arrival estimation using non-parametric statistics. IEEE Trans. Signal Process. **49**(9), 2060–2073 (2001)

Publisher's Note